Micromechanical model for anisotropic rock joints

Anil Misra

Micromechanical model for anisotropic rock joints

Anil Misra

Department of Civil Engineering, University of Missouri, Kansas City

Abstract. Force-deformation relationships of rock joints are important in the study of mechanical behavior of fractured or jointed rocks. Experimental studies have shown that rock joints often exhibit deformation hardening and anisotropic behavior under shearing loads. This paper focuses upon the mathematical modeling of force-deformation behavior of anisotropic rock joints by explicitly considering interaction of asperities on a joint surface. Elastic deformations and inelastic frictional sliding are considered at inclined asperity contacts. A modified spherical harmonic expansion is introduced to model the orientation distribution of asperity contacts. The resultant joint force-deformation model is used to obtain the normal and shear stiffness behavior of anisotropic joints. Results obtained from the model show that the asperity contact orientation distribution is essential for representing the anisotropic nature of interface geometry and for modeling deformation hardening of interfaces. The model results are compared with experimental data culled from the literature.

1. Introduction

The geophysical behavior of many geological materials, such as jointed rocks, gravel, and sand, depend significantly on the behavior of block or particle interfaces. In the field of interface behavior, Hertz pioneered the study of effects produced by mutual compression of nonconforming elastic bodies by considering the case in which forces were normal to a perfectly smooth interface surface. Although perfectly smooth surfaces provide an important starting point in the study of interface behavior, they seldom represent realistic situations. The mechanical behavior of rock joints is more complex and influenced by a great variety of factors, such as rock elastic properties, mineral friction, surface adhesion, surface topography, and the presence of fluids and debris at the interface. A number of studies have been published since the pioneering work by Hertz that have aimed to address more realistic interfaces [*Johnson*, 1985; *Hills et al.*, 1992]. Within the context of contact theories, the present work considers the behavior of rock joints by explicitly modeling the influence of joint surface topography. The intent is to develop force-deformation relationships for rock joints that may be used in the mechanistic modeling of highly fractured rocks and granular materials [*Misra*, 1995].

In their study of friction between solid surfaces, *Bowden and Tabor* [1950] had recognized that the actual contact area at the interface is smaller than the area of contacting surface, and the actual contact area depends on the normal loading condition. The smaller contact area is a manifestation of the fact that at the interface of rough surfaces, the actual contact is between the asperities on the surfaces. Thus the force-deformation behavior of the interface is determined by the behavior of asperity contacts. *Archard* [1957] considered the contact between asperities in a paper dealing with the elastic deformation and friction laws of a contacting rough surface and rigid plane. Along these lines, considering asperity contacts to be Hertzian in nature and using Gaussian distributions of surface heights, *Greenwood and Williamson* [1966] derived a model for the mechanical behavior of a rough surface contacting a rigid plane. The Greenwood-Williamson model was subsequently extended by J.A. Greenwood and coworkers to study the behavior of contacting rough surfaces under normal loads [see *Hills et al.*, 1992, chapter 14]. Since then, the normal contact of rough surfaces has been widely studied [see *Swan*, 1983; *Brown and Scholz*, 1985, 1986]. Models of contacting rough surfaces under normal loads have also been developed by treating the asperities to be elliptical paraboloids [*Bush et al.*, 1975; *O'Callaghan and Cameron*, 1976]. These models have been used to simulate isotropic as well as anisotropic interface surfaces by accounting for aspect ratios and principal axis orientations of elliptical paraboloid asperities [*Bush et al.*, 1978; *McCool and Gassel*, 1981; *McCool*, 1986]. The plasticity of asperity contacts has been considered in the context of the Greenwood-Williamson approach [see *Chang et al.*, 1987]. Furthermore, the analysis of Greenwood and Williamson has been extended to study the normal and shear behavior of contacting rough surfaces under elastic deformation of asperity contacts [*Yamada et al.*, 1978; *Swan and Zongqi*, 1985; *Yoshioka and Scholz*, 1989a, b]. More recent studies have considered the sliding at asperity contact with the aim of obtaining friction behavior of contacting rough surfaces [*Boitnott et al.*, 1992; *Ford*, 1993, *Misra*, 1997]. *Yoshioka* [1997] provides a review of some of the recent micromechanical methods.

In the present paper, we develop a kinematically driven micromechanical methodology for contacting rough surfaces that considers oblique asperity contacts. We introduce a directional distribution function of asperity contact orientations, recognizing that the asperity contacts are not equally likely in all directions. In addition, we utilize an iterative procedure to obtain the asperity contact forces at each load increment, recognizing that the asperity contact force distribution is not always known a priori. Furthermore, in the model derivation the normal and shear behavior of the interface are considered together. Therefore the resultant

Paper number 1999JB900210.
0148-0227/99/1999JB900210$09.00

model naturally accounts for the coupling between normal and shear behavior of rough joints, even though at asperity contact level, there is no such coupling. Also, the effects of asperity contact loss and formation of new asperity contacts during shear loading are explicitly modeled. The developed micromechanical methodology is used to (1) model the anisotropy of interfaces under shear loading and (2) replicate the deformation hardening of interface shear resistance under shear loading. This endeavor is motivated by experimental results on (1) directional dependence of interface friction and shear stiffness presented by *Jing et al.* [1992] and (2) the shear hardening behavior measured by *Biegel et al.* [1992].

In the discussion that follows we first present a description of the modeling methodology as it pertains to the force-deformation relationship of an interface. The derived interface force-deformation relationship is subsequently used to study interface behavior for a variety of asperity contact behavior and loading conditions. The predictions of the derived model are compared with experimental data from the literature.

2. Micromechanical Constitutive Relation of Interface

We consider the interface force-deformation behavior of contacting surfaces, which contact via asperties as shown in Figure 1. As schematically depicted in Figure 1, we develop a micromechanical methodology, wherein the force-deformation behavior of the interface is obtained by considering the force-deformation behavior of the asperity contacts. At the asperity contact level, a local force-deformation relationship is defined that accounts for the elastic deformation and inelastic sliding at the contact. Finally, an overall interface force-deformation relationship is derived, accounting for (1) the geometry of the asperity contacts and (2) the kinematic constraints and equilibrium conditions for the interface.

2.1. Asperity Behavior

The interaction at an asperity contact is assumed to be a Hertz-Mindlin type contact of perfectly smooth interface. Under an arbitrary motion of the interacting surfaces the relative motion δ_j^c at an asperity contact may be decomposed, in general, into an elastic part δ_j^{ce} and an inelastic part δ_j^{cp}, such that

$$\delta_j^c = \delta_j^{ce} + \delta_j^{cp}. \tag{1}$$

Subscripts follow the established tensor convention unless specified otherwise. Considering smooth sliding at an enduring asperity contact and neglecting any plastic deformations in the normal direction, the inelastic part of relative motion δ_j^{cp} is expressed by

$$\delta_j^{cp} = \gamma^c \zeta_j^c, \tag{2}$$

where γ^c is the magnitude of the inelastic motion and ζ_j^c is the unit vector along the sliding direction.

The force generated by the relative displacement at an asperity contact is related via the asperity contact stiffness K_{ij}^c as follows

$$f_i^c = K_{ij}^c \delta_j^{ce} \tag{3}$$

or, from equations (1) and (2)

$$f_i^c = K_{ij}^c \left(\delta_j^c - \gamma^c \zeta_j^c \right). \tag{4}$$

We note that the asperity contact stiffness K_{ij}^c generally depends upon the contact loading condition, such as the stiffness given by the Hertz-Mindlin contact theory. In the following derivation we make no assumption regarding the form of this dependency. Later in the paper, we utilize both constant and nonconstant asperity contact stiffnesses for our parametric studies.

At an asperity contact, Amonton-Coulomb's friction law, expressed by the following inequality, governs sliding:

$$f_i^c q_i^c \le 0, \tag{5}$$

where

$$q_i^c = \zeta_i^c + \mu \; n_i^c, \tag{6}$$

where μ is the asperity friction coefficient and n_i^c is a vector normal to the asperity contact. It follows from equations (4) and (5) that at the point of impending sliding at an asperity contact,

$$K_{ij}^c \left(\delta_j^c - \gamma^c \zeta_j^c \right) q_i^c = 0, \tag{7}$$

which yields the following expression for the magnitude of inelastic motion γ^c in terms of the relative motion, δ_j^c:

$$\gamma^c = \left(M^c K_{ij}^c q_i^c \right) \delta_j^c, \tag{8}$$

where the scalar M^c is given by

$$M^c = \left(K_{ij}^c \zeta_j^c \, q_i^c \right)^{-1}. \tag{9}$$

Thus, equations (4) and (8) lead to the following relationship between the force and relative motion at a sliding asperity contact:

$$f_i^c = K_{ir}^c \left(\delta_{rj} - M^c K_{sj}^c q_s^c \zeta_r^c \right) \delta_j^c, \tag{10}$$

where δ_{rj} ($\delta_{rj} = 1$ for $r = j$ and $\delta_{rj} = 0$ for $r \neq j$) is the Kronecker delta.

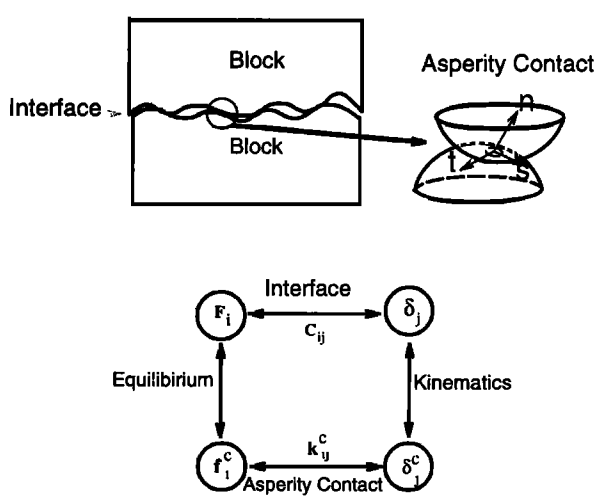

Figure 1. Schematic depiction of the micromechanical modeling methodology for interfaces.

2.2. Interface Behavior

The geometry of an interface determines the orientations and the number of asperity contacts under a given loading condition. From the viewpoint of modeling interface behavior

the geometry of composite topography of contacting surfaces has been found to be more applicable [*Francis*, 1977; *Brown and Scholz*, 1985]. For a given resolution the composite topography may be reasonably described via statistics of asperity contact height, curvature, and orientation [*Nayak*, 1971; *Adler and Firman*, 1981]. In general, these parameters are not independent of each other, and therefore their distribution functions may not be formulated independently. Nevertheless, the derivation of a force-deformation relationship is considerably simplified by considering these parameters independently. In this paper, we assume the distributions of asperity contact heights, curvatures, and orientations to be independent of each other. In the subsequent discussions the asperity contact curvatures are taken to be uniform. Only distributions of asperity contact heights and orientations are considered in the derivations and examples presented thereafter. While the forms of distribution functions of asperity heights are known on the basis of topography measurements of rough surfaces, the distribution function of asperity contact orientation is introduced here for the first time.

2.2.1. Asperity heights. It is convenient to interpret the asperity contact height with reference to the highest peak of the composite topography as shown in Figure 2. Given that the total number of asperities per unit area at an interface is N and $H(r)$ is a probability density function, then $N\,H(r)\,dr$ denotes the number of asperity contacts in the interval represented by r and $r+dr$. Here r denotes the overlap of the interacting asperities under a given interface force or displacement. It follows that the number of asperity contacts under this force or displacement is given by

$$N_r = \int_0^r N\,H(r)\,dr. \tag{11}$$

The experimental measurements of topography suggest a skewed distribution for asperity heights, and several statistical distributions, such as chi-square distribution and gamma distribution, have been used to model rough surfaces [see *Adler and Firman*, 1981; *Yoshioka and Scholz*, 1989a]. In this paper, we use a gamma distribution for simplicity. However, it is noteworthy that a chi-square distribution provides a more versatile representation. For a gamma distribution of asperity heights the density function $H(r)$ is expressed as

$$H(r) = \frac{r^{\alpha}\, e^{-r/\beta}}{\Gamma(\alpha+1)\beta^{\alpha+1}} \quad (0 < r < \infty,\ \alpha > -1,\ \beta > 0), \tag{12}$$

where α and β are parameters related to the mean and variance of the asperity heights as follows

$$\begin{aligned} &\text{Mean} && r_m = \beta(\alpha+1) \\ &\text{Variance} && r_\sigma^2 = \beta^2(\alpha+1). \end{aligned} \tag{13}$$

Parameter α is unitless, while parameter β takes the unit of asperity height. Figure 3 illustrates the distribution of asperity heights for smooth and rough surfaces on the basis of data from *Yoshioka and Scholz* [1989a] on Westerly granite. From the viewpoint of asperity heights, interfaces with narrow distributions of asperity heights are considered smooth, while interfaces with broad distributions of asperity heights are considered rough. In Figure 3 the measured asperity height distribution is denoted by solid circles and the best fit gamma distribution is represented by a curve with following parameters: $\alpha = 3.82$ and $\beta = 1.15$ μm for a smooth interface and $\alpha = 6.14$ and $\beta = 3.52$μm for a rough interface. The measured height distributions may be different from the actual distribution depending on the resolution of the topography measurements. *Yoshioka and Scholz* [1989a] have devised a method for relating measured and actual asperity height distributions. In any case, the shapes of the distributions are qualitatively similar. Therefore, in this paper, we use a gamma distribution as given in equation (12).

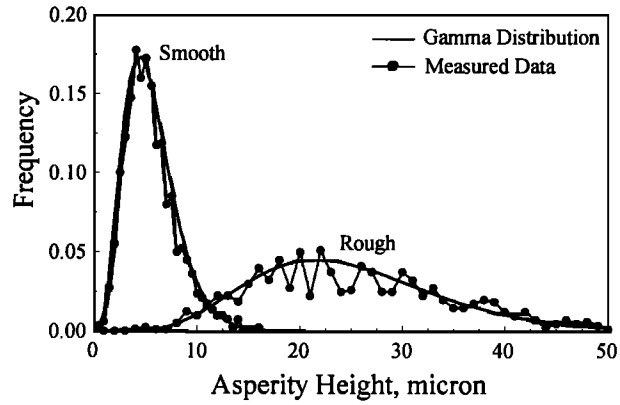

Figure 3. Asperity height distributions for a smooth interface and a rough interface.

2.2.2. Asperity contact orientations. At an interface, asperity contacts may occur in various directions. Asperity contact orientation may be defined by considering the inclination of the asperity contact normal with respect to that of interface normal direction. Figure 4 shows an oblique asperity contact whose orientation is defined by the azimuthal angle ϕ and the meridional angle θ, measured with respect to a Cartesian coordinate system in which direction 1 is normal to the interface. Thus the frequency distribution of asperity contact orientation requires a density function in spherical

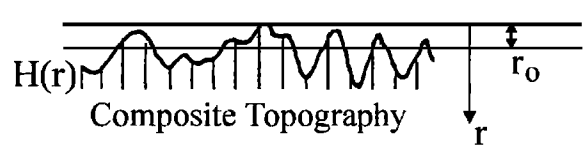

Figure 2. Depiction of composite topography.

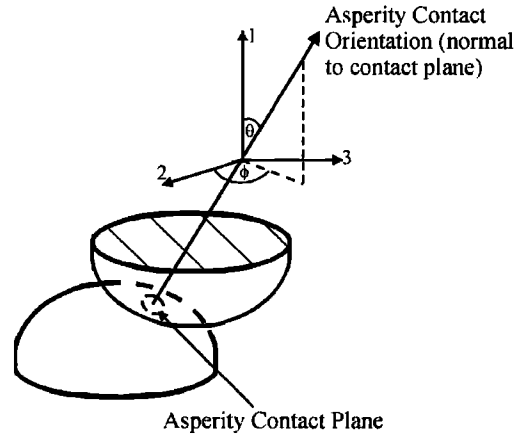

Figure 4. Asperity contact orientation.

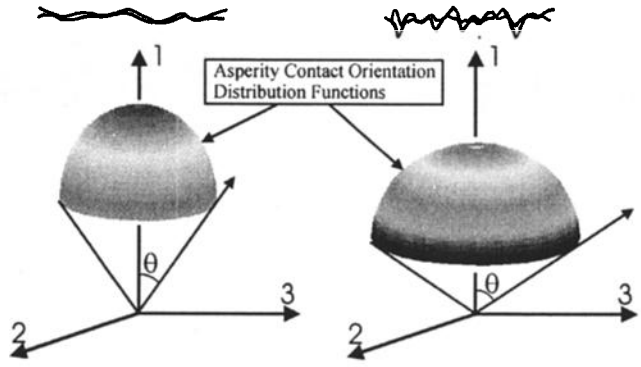

Figure 5. Schematic depiction of asperity contact orientation distri-bution functions for smooth and rough interfaces.

polar coordinates, which can describe the concentrations of asperity contact orientations. Furthermore, the density function should be able to model a variety of joints ranging from those that may be considered smooth to those considered rough. As illustrated in Figure 5, the asperity contact of smooth joints has a greater tendency to concentrate in the direction normal to the interface than that of rough joints. In particular, a perfectly smooth interface will have a single contact in the normal direction, while a very rough surface is likely to have asperity contact orientations in all directions. Spherical harmonics expansions may be used to represent these asperity contact orientation distributions [*Chang and Misra*, 1989]. Here we use a modified form of spherical harmonics expansion to represent the asperity contact distribution for rock joints ranging from smooth to rough. Considering the first two terms of spherical harmonics expansion in the domain; $0 \le \theta \le 2\pi/a$, and $0 \le \phi \le 2\pi$, the density function $\xi(\Omega)$ of directional distribution of asperity contacts is expressed by

$$\xi(\Omega) = \frac{a \sin a\theta}{2\pi \sin\theta}\left[1 + \frac{b}{4}\left(3\cos 2a\theta + 1\right) + 3c \sin^2 a\theta \cos 2\phi\right] \quad (14)$$

$$\left(0 \le \theta \le \frac{\pi}{2a};\quad 0 \le \phi \le 2\pi;\quad a \ge 1\right),$$

where angles ϕ and θ are defined in Figure 6 and Ω represents the solid angle formed by ϕ and θ. Parameters a, b, and c determine the shape of the density function $\xi(\Omega)$. Higher-order terms may be considered to represent more complex orientation distributions; however, terms included in equation (14) are adequate to model the anisotropy of an interface. It is a matter of straightforward calculation to show that the density function $\xi(\Omega)$ satisfies the condition

$$\int_0^{2\pi} \int_0^{\pi/2a} \xi(\phi, \theta) \sin\theta \, d\theta \, d\phi = 1. \quad (15)$$

Thus the product $N_r\, \xi(\Omega)\, d\Omega$ denotes the number of asperity contacts N_Ω in the interval represented by solid angles Ω and $\Omega + d\Omega$, that is

$$N_\Omega = N_r\, \xi(\Omega)\, d\Omega. \quad (16)$$

The mean and variance of asperity contact orientations in the meridional directions may be obtained as the expectations $E[\theta] = \int \theta \xi(\Omega)\, d\Omega$ and $E[(\theta - E[\theta])^2] = \int (\theta - E[\theta])^2\, \xi(\Omega)\, d\Omega$, given by

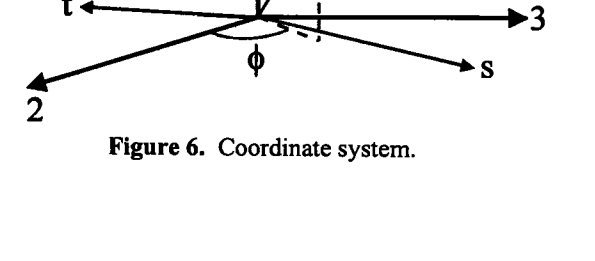

Figure 6. Coordinate system.

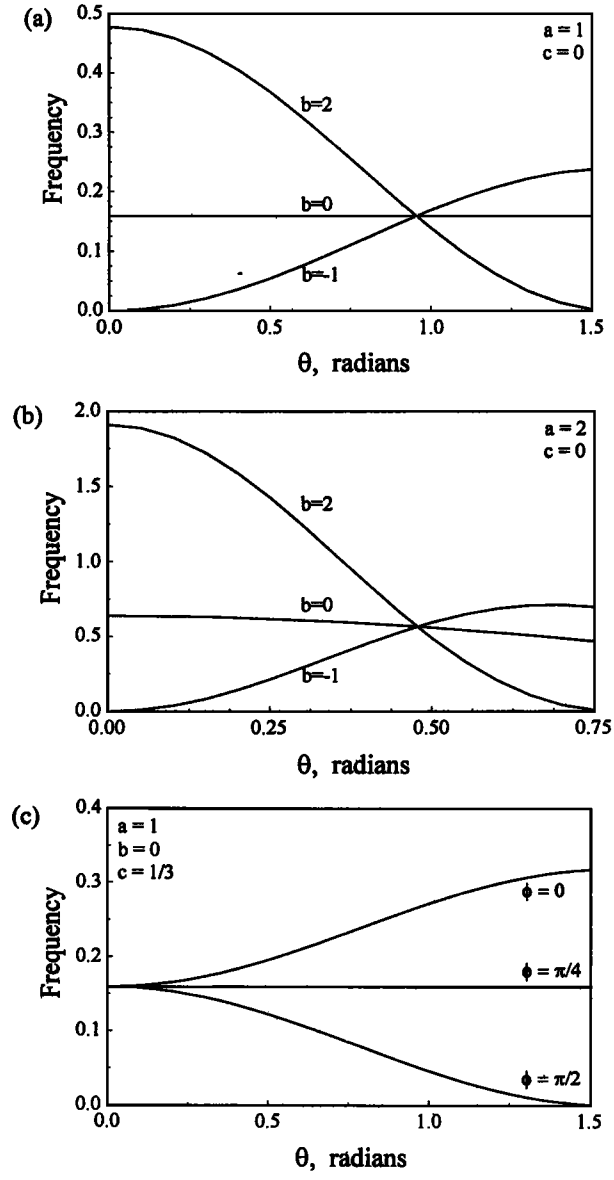

Figure 7. Dependence of asperity contact orientation distribution on parameters a, b, and c.

$$E[\theta]=\frac{6-b}{6a}$$
$$E\left[(\theta-E[\theta])^2\right]=\frac{36\pi-108+20b-6b\pi-b^2}{36a^2}. \quad (17)$$

Furthermore, to ensure that the density function $\xi(\Omega)$ is positive semidefinite, $\xi(\Omega) \geq 0$, the values of parameters b and c are bounded as follows:

$$-1 \leq b \leq 2 \qquad -\frac{1}{3}+\frac{b}{6} \leq c \leq \frac{1}{3}-\frac{b}{6}. \quad (18)$$

The asperity contact orientation parameters a and b model the influence of joint roughness on asperity contact orientation. It is noteworthy that as parameter a increases, the contact distribution concentrates toward the direction normal to the interface. For example, the density function $\xi(\Omega)$ behaves like a delta function in the limit $a \rightarrow \infty$ and yields an expectation $E[\theta] = 0$, representing a concentrated contact orientation, normal to the interface of a perfectly smooth joint. Thus parameter a describes the extent of the asperity contacts in the meridional direction. Parameter b, on the other hand, describes the shape of the contact distributions within the meridional extent of asperity contacts. As illustrated in Figures 7a and 7b, the extent of asperity contact inclination in meridional direction is $\pi/2$ for $a = 1$ and $\pi/4$ for $a = 2$, while, the shapes of contact distributions vary with the values of parameter b. Parameter $b = -1$ represents an interface on which the asperity contacts tend to orient closer to the horizon, i.e. $\theta = \pi/2$. In contrast, parameter $b = 2$ represents an interface on which preferred orientation is closer to the interface normal, i.e., $\theta = 0$. For $b = 0$ the asperity contacts are equally distributed in the meridional direction. The asperity contact orientation parameter c models the directional nature of roughness on the joint surface and is appropriate for modeling anisotropy of joint roughness in the azimuthal direction. Figure 7c, which gives a plot of the asperity contact distributions at various azimuthal angles ϕ for parameters $a = 1$, $b = 0$, and $c = 1/3$ illustrates the anisotropy of asperity contact orientations. For parameter $c = 0$, isotropic asperity contact distribution is obtained in the azimuthal direction.

2.2.3. Force-deformation relationship. Considering the equilibrium of two interacting rock blocks, the overall force F_i at the rock joint is the summation of the forces f_i^c developed at asperities, that is

$$F_i = \sum_c f_i^c. \quad (19)$$

For a large number of asperity contacts the summation may be replaced by the following integration accounting for the distributions of asperity contact heights and orientations:

$$F_i = N \int_r \int_\Omega f_i^c \xi(\Omega) H(r)\ d\Omega\ dr, \quad (20)$$

where overall force F_i is given as force per unit area since N is measured per unit area of a joint.

Under a given loading condition an asperity contact may be sliding, separated, or in elastic contact. Appropriately accounting for the asperity contact forces and adopting the kinematic assumption that relative motion at an asperity δ_j^c is same as the relative motion of the interface δ_j the relationship between the overall force F_i at the joint and the relative motion δ_j may be written as

$$F_i = C_{ij}\delta_j = \left[\ C_{ij}^e - C_{ij}^p\ \right]\delta_j, \quad (21)$$

where the superscripts e and p refer to the elastic and inelastic part of the interface stiffness tensor C_{ij}. The elastic part C_{ij}^e, which is independent of the asperity contact sliding or separation, is given by

$$C_{ij}^e = N \int_r \int_\Omega K_{ij}^c \xi(\Omega) H(r)\, d\Omega\, dr, \quad (22)$$

where the integration is performed over all the asperity contacts at the interface specified by the distributions of asperity contact orientations and asperity heights under a given interface normal load.

On the other hand, the inelastic part depends critically on the asperity contact loading condition. During an arbitrary shear loading the inelastic part has two contributions: (1) from asperity contact sliding, and (2) from separation of asperity contacts. It is expected that some of the oblique asperity contacts that are in contact under an initially applied normal load undergo unloading as the interface is sheared. These contacts could potentially separate during the shear loading. Accounting for the two mechanisms of inelastic deformation, the inelastic part of the interface stiffness tensor C_{ij}^p is given by

$$C_{ij}^p = N \int_{r^s} \int_{\Omega^s} M^c K_{ik}^c \zeta_k^c K_{nj}^c q_m^c \xi(\Omega) H(r)\, d\Omega\, dr + N \int_{r^d} \int_{\Omega^d} K_{ij}^c \xi(\Omega) H(r)\, d\Omega\, dr, \quad (23)$$

where the integration is performed over the domain of sliding asperity contacts denoted by superscript s and separated asperity contacts denoted by superscript d.

3. Rock Joint Behavior for Constant Asperity Stiffness

Since the domain of sliding and separated asperity contacts is not always known a priori, numerical effort is typically required to evaluate the integrals in equations (22) and (23). Nevertheless, under certain simple loading conditions and for linear asperity contacts the integrals in equations (22) and (23) may be evaluated in closed forms to obtain analytical expressions of interface stiffness. For the subsequent derivation it is convenient to express the asperity stiffness tensor K_{ij}^c in terms of asperity stiffness that describes the behavior along the direction of normal and tangent to an asperity contact, such that

$$K_{ij}^c = K_n^c n_i^c n_j^c + K_s^c \left(s_i^c s_j^c + t_i^c t_j^c\right), \quad (24)$$

where K_n and K_s denote asperity stiffness along the normal and tangential direction of the asperity. It is assumed that the stiffness term that cross-links normal and shear behavior is negligible. The unit vector $\mathbf{n}$ is normal to the asperity contact surface and vectors $\mathbf{s}$ and $\mathbf{t}$ are arbitrarily chosen on the plane tangential to the asperity contact surface, such that $\mathbf{nst}$ forms a local Cartesian coordinate system, as illustrated in Figure 6. The vectors $\mathbf{n}$, $\mathbf{s}$, and $\mathbf{t}$ used in this paper are given by

$$\begin{aligned} \mathbf{n} &= \langle\ \cos\theta,\ \sin\theta\cos\phi,\ \sin\theta\sin\phi\ \rangle \\ \mathbf{s} &= \langle\ -\sin\theta,\ \cos\theta\cos\phi,\ \cos\theta\sin\phi\ \rangle \\ \mathbf{t} &= \langle\ 0,\ -\sin\phi,\ \cos\phi\ \rangle. \end{aligned} \quad (25)$$

3.1. Elastic Behavior

The elastic part of the interface stiffness may be obtained by integrating equation (22). For simplicity of derivation, we

Table 1. Analytical Expressions for Elastic Interface Stiffness

Parameter a	C_{11}/N	C_{22}/N	C_{33}/N
1	$\frac{1}{3}(K_n+2K_s)+\frac{2b}{15}(K_n-K_s)$	$\frac{1}{3}(K_n+2K_s)-\frac{b}{15}(K_n-K_s)+\frac{2c}{5}(K_n-K_s)$	$\frac{1}{3}(K_n+2K_s)-\frac{b}{15}(K_n-K_s)-\frac{2c}{5}(K_n-K_s)$
2	$\frac{1}{4}(3K_n+K_s)+\frac{b}{16}(K_n-K_s)$	$\frac{1}{8}(K_n+7K_s)-\frac{b}{32}(K_n-K_s)+\frac{5c}{32}(K_n-K_s)$	$\frac{1}{8}(K_n+7K_s)-\frac{b}{32}(K_n-K_s)-\frac{5c}{32}(K_n-K_s)$
3	$\frac{1}{5}(7K_n-2K_s)-\frac{3\sqrt{3}}{10}(K_n-K_s)+\frac{(69\sqrt{3}-72)b}{1540}(K_n-K_s)$	$-\frac{1}{5}(K_n-6K_s)+\frac{3\sqrt{3}}{20}(K_n-K_s)-\frac{(531\sqrt{3}-688)c}{3080}(K_n-K_s)$	$-\frac{1}{5}(K_n-6K_s)+\frac{3\sqrt{3}}{20}(K_n-K_s)+\frac{(531\sqrt{3}-688)c}{3080}(K_n-K_s)$
8	K_n	K_s	K_s

consider uniform asperity heights, thus equation (22) is reduced to

$$C_{ij}^{e} = N \int_0^{2\pi} \int_0^{\pi/2a} K_{ij}^{c}\, \xi(\phi,\theta) \sin\theta \; d\theta \; d\phi, \qquad (26)$$

where the asperity orientation density function $\xi(\Omega)$ is given in equation (14). Since the general form of the analytical expressions is quite complex, particular expressions for roughness parameter a = 1, 2, 3, and ∞ are given in Table 1. It is noted that the terms that cross-link the normal and shear stiffness, namely C_{ij}^{e} (i ≠ j), are identically zero. It is also noteworthy that as the parameter a tends toward infinity; that is, as the asperity contacts tend to align in a direction normal to the interface the interface stiffness tensor C_{ij}^{e} becomes proportional to that of a single asperity contact. Given that the asperity contact density N = 1 for a perfectly smooth interface, the interface stiffness C_{ij}^{e}, at a = ∞, correctly reduces to the asperity stiffness.

The closed-form relationships in Table 1 also give the effect of parameters b and c on the interface elastic stiffness. These effects are illustrated in Figures 8 and 9 for parameters b and c and various asperity stiffness ratios K_s/K_n. Figure 8a gives a plot of the interface stiffness ratio C_{22}/C_{11} versus asperity contact orientation parameter a for the limiting values of parameter b = -1 and 2 when c = 0, and an asperity stiffness ratio K_s/K_n = 0.5. As expected the interface stiffness ratio

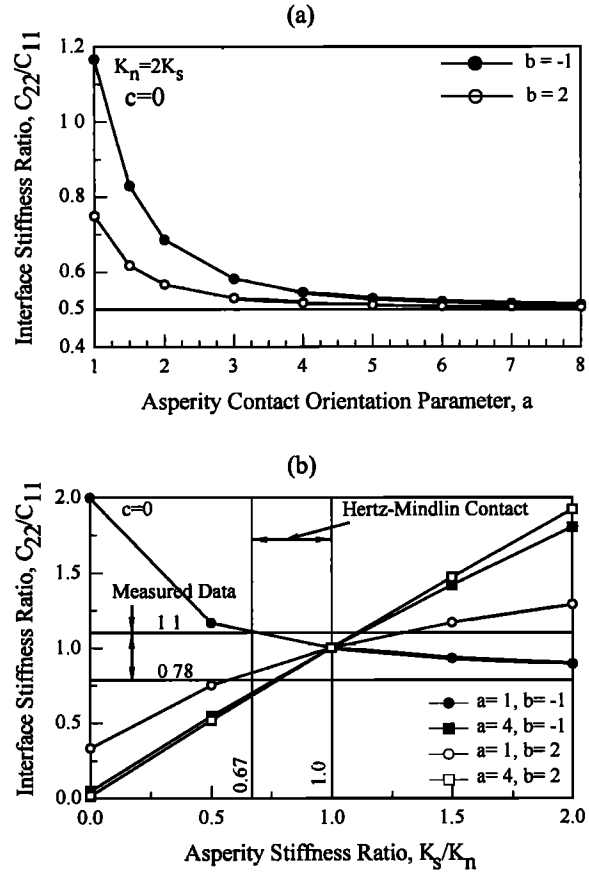

Figure 8. Relationship of interface elastic stiffness ratio with (a) asperity orientation parameter a and (b) asperity stiffness ratio K_s/K_n.

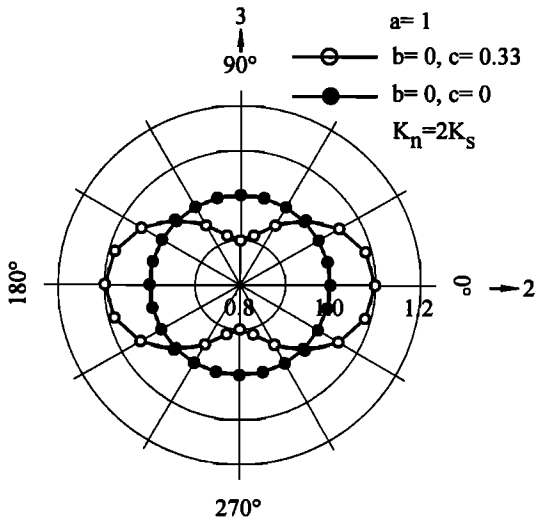

Figure 9. Directional dependency of interface elastic stiffness ratio C_s/C_{11} on asperity orientation parameters b and c for asperity stiffness ratio $K_s/K_n = 0.5$.

tends toward the asperity stiffness ratio as the asperity contact orientations align in the direction normal to the interface.

Interestingly, interface stiffness ratio $C_{22}/C_{11} > 1$ is obtained for certain interface geometry even when the asperity stiffness ratio $K_s/K_n = 0.5$. Physically, this means that under vanishing interface shear forces, such that elastic conditions may be assumed, the interface is stiffer in the tangential direction compared to the normal direction. Higher shear stiffnesses are possible for interfaces on which a preponderance of asperity contacts are oriented closer to the horizon as opposed to the direction normal to the interface. Asperity contact orientation distribution for $b = -1$ in Figure 7 represents an interface on which most of the asperity contacts are inclined at meridional angle $\theta > 45°$. It is noteworthy that experimental measurements of interface stiffness ratio C_{22}/C_{11} reported by *Krolikowski and Szczepek* [1993], under elastic conditions using an ultrasonic technique, range from 1.1 to 0.78. The measured ratios have no discernible dependence upon the normal pressure and display some scatter.

It is instructive to compare the interface stiffness ratio with the likely asperity contact stiffness ratio for an asperity contact. Assuming that the asperity stiffness is given by the Hertz-Mindlin contact theory for perfectly smooth interface, the following ratio is obtained for elastic contact [*Mindlin and Deresiewicz*, 1953; also see *Misra*, 1995]:

$$\frac{K_s}{K_n} = \frac{2(1-\nu)}{2-\nu}, \tag{27}$$

yielding an asperity contact stiffness ratio ranging from 1 to 0.67 for Poisson's ratio ν ranging from 0 to 0.5. For quartz, with a Poisson's ratio of 0.3, the asperity contact stiffness ratio will be 0.83. Thus it is natural to conclude that the measured stiffness ratio in the range 1.1 to 0.78 for a rough quartz interface is a consequence of the asperity contact orientation distribution. The present model reasonably accounts for this effect of the interface geometry. The influence of asperity contact orientation parameters a and b on interface behavior is further illustrated in Figure 8b, which gives a plot of the interface stiffness ratio versus the asperity contact stiffness ratio. Horizontal lines at ratios 1.1 and 0.78 show the range of the interface stiffness ratios measured by *Krolikowski and Szczepek* [1993]. Vertical lines at ratios 0.67 and 1.0 show the range of asperity contact stiffness ratios predicted on the basis of Hertz-Mindlin contact theory for perfectly smooth. Interface stiffness ratios calculated using the present model are also plotted for a selected values of parameters a and b.

The asperity contacts orientation parameter c models the anisotropy of asperity contact orientation distribution as shown previously in Figure 7. To examine the effect of asperity contact orientation anisotropy, we consider the resultant interface shear stiffness C_s, which is defined as

$$C_s = \sqrt{C_{22}^2 \cos^2\phi + C_{33}^2 \sin^2\phi}, \tag{28}$$

where ϕ is the azimuthal angle defined on the plane normal to the interface as shown in Figure 6. Figure 9 gives a polar plot of the interface shear stiffness ratio C_s/C_{11} for asperity contact orientation parameter $a = 1$, $b = 0$, and $c = 1/3$ and 0. For parameter $c = 1/3$, more asperity contacts are aligned along direction 2 ($\phi = 0°$) as opposed to direction 3 ($\phi = 90°$). Consequently, the shear stiffness is higher along direction 2 ($\phi = 0°$) as opposed to direction 3 ($\phi = 90°$). For parameter $c = 0$ the interface asperity contact distribution is isotropic, hence the resultant shear stiffness is isotropic as shown by the circle in Figure 9.

3.2. Inelastic Behavior Under Normal Loading

For normal deformation of an interface, such that $\delta_1 = \delta$, and $\delta_2 = \delta_3 = 0$, the sliding at asperity contacts is the sole contributor to the inelastic part of the stiffness tensor C_{ij}^p. In this case, the sliding direction at an asperity contact is given by the vector **s** defined in equation (25), so that $\zeta_j^c = s_j^c$, and the sliding domain may be denoted by $0 \le \phi \le 2\pi$ and $\theta_s \le \theta \le \pi/2a$, indicated by the dark shaded area in Figure 10. Now, considering, for simplicity, the case of uniform asperity heights, the inelastic part of the interface stiffness tensor C_{ij}^p may be obtained as

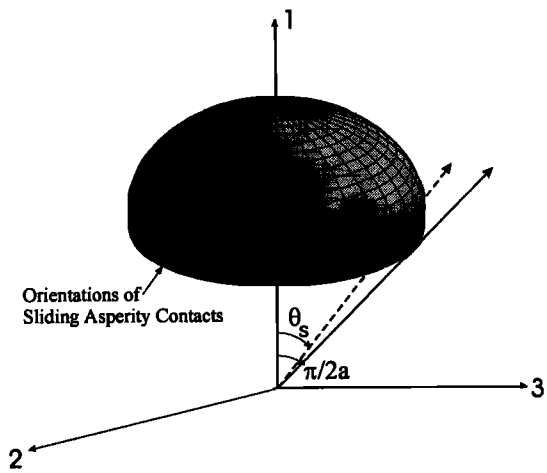

Figure 10. Asperity contact orientation distribution function showing the orientation of sliding asperity contacts.

Table 2. Analytical Expressions for Inelastic Interface Stiffness Under Normal Deformation

Parameter a	C_{11}^p/N	$C_{22}^p/N = C_{33}^p/N$
1	$\frac{1}{3}\mu K_n\left(\sin^3\theta_s - 1\right)+\frac{1}{3}K_s\cos\theta_s\left(3-\cos^2\theta_s\right)$	$\frac{1}{6}\mu K_n\left(1-\sin^3\theta_s\right)+\frac{1}{6}K_s\cos^3\theta_s$
2	$\frac{1}{8}\mu K_n\left(4\theta_s-\pi-\sin 4\theta_s\right)+\frac{1}{8}K_s\left(4\cos 2\theta_s-\cos 4\theta_s-1\right)$	$\frac{1}{16}\mu K_n\left(\pi+\sin 4\theta_s-4\theta_s\right)+\frac{1}{16}K_s\left(4\cos 2\theta_s+\cos 4\theta_s+1\right)$
∞	0	K_s

$$C_{ij}^p = N\int_0^{2\pi}\int_{\theta_s}^{\pi/2a} M^c K_{ik}^c \zeta_k^c K_{nj}^c q_m^c \xi(\phi,\theta)\sin\theta\, d\theta\, d\phi, \quad (29)$$

where the asperity orientation density function $\xi(\Omega)$ is given in equation (14).

For constant asperity stiffnesses K_n and K_s that are independent of asperity force or displacement the sliding domain is obtained using the Amonton-Coulomb friction law in equation (5) along with equation (4) as $0 \le \phi \le 2\pi$ and $\theta_s \le \theta \le \pi/2a$, where

$$\theta_s = \arctan\left(\frac{\mu K_n}{K_s}\right) \quad (30)$$

and μ is the asperity friction coefficient. It is noteworthy that sliding at an asperity contact is not only governed by the asperity friction coefficient but also by the ratio of normal and tangential asperity stiffness.

Now, integrating equation (29), closed-form expressions for the inelastic part of the interface stiffness may be obtained. For isotropic interfaces, with asperity contact orientation parameter $b = c = 0$, expressions for the inelastic part of interface stiffness are tabulated in Table 2 for roughness parameter $a = 1$, 2, and ∞. It is noted that the cross-linking term that links the shear and normal behaviors is identically zero, i.e. $C_{12}^p = C_{13}^p = C_{23}^p = 0$.

Furthermore, for frictionless asperity contact, i.e., $\mu = 0$ and, consequently, $\theta_s = 0$, the expressions for the inelastic part of normal stiffness tensor C_{11}^p reduce to

$$C_{11}^p = \frac{2K_s}{3} \quad a = 1 \qquad C_{11}^p = \frac{K_s}{4} \quad a = 2. \quad (31)$$

As expected, for this case, the normal interface stiffness C_{11} is independent of asperity shear stiffness K_s given by

$$C_{11} = \frac{K_n}{3} \quad a = 1 \qquad C_{11} = \frac{3K_n}{4} \quad a = 2. \quad (32)$$

It is also noteworthy that as asperity contact orientation parameter a tends to infinity the inelastic part of normal interface stiffness C_{11}^p vanishes. Thus for parameter $a = \infty$ the normal interface stiffness C_{11} is proportional to normal asperity stiffness K_n.

4. Rock Joint Behavior for Nonconstant Asperity Stiffness

As seen from section 3, constant asperity stiffness yields closed-form analytical solutions and initial estimates of interface behavior, albeit under restrictive conditions. For modeling the rock joint behavior under general loading conditions, nonconstant asperity contact stiffnesses, that depend upon contact forces or displacements are preferable. Considering the Hertz-Mindlin contact theory of perfectly smooth elastic interfaces as well as other theories of elastic-plastic interfaces [see *Johnson,* 1985], it is reasonable to assume that the normal asperity stiffness K_n depends on the normal asperity deformation δ_n according to the following power law:

$$K_n = \lambda K \delta_n^{\eta}, \quad (33)$$

where K, λ, and η are constants. The asperity stiffness K_n given by equation (33) becomes identical to the Hertz-Mindlin stiffness for contact of perfectly smooth elastic spheres when

$$\lambda = \frac{2-\nu}{2(1-\nu)} \quad \eta = \frac{1}{2} \quad K = \frac{8G\sqrt{R}}{3(2-\nu)}, \quad (34)$$

where G is the shear modulus, ν is Poisson's ratio, and R is asperity radius of curvature. It is noteworthy that the exponent η can vary from 0 for perfectly plastic to ½ for perfectly elastic behavior at contact of perfectly smooth spherical asperities [*Johnson,* 1985].

The tangential asperity stiffness K_s has, in general, a complex dependence on the asperity loading conditions in the tangential direction as exemplified by the study of *Mindlin and Deresiewicz* [1953] on perfectly smooth elastic spheres subjected to varying normal and tangential forces. Since this paper focuses on monotonic loading of interfaces, we consider the case of constant normal asperity force and monotonically increasing asperity shear force. Mindlin and Deresiewicz have derived the following asperity force-displacement relationship for this loading condition, considering partial slip at contact edge with increasing contact shear displacement:

$$f_s = \mu K_n \delta_n \left[1-\left(1-\frac{\delta_s}{\mu\lambda\delta_n}\right)^{3/2}\right], \quad (35)$$

where f_s is the asperity shear force and δ_n and δ_s are the asperity normal and shear displacements, respectively. It can be shown that in this case, the tangential asperity stiffness K_s varies from $3K_n/2\lambda$, for vanishingly small asperity shear force, to K_n/λ, for asperity shear force at incipient sliding condition given by equation (5). In this paper, we use the following truncated series representation for the tangential asperity stiffness K_s:

$$K_s = \frac{3K_n}{2\lambda}\left[1-\frac{1}{4\mu\lambda}\frac{\delta_s}{\delta_n}-\frac{1}{24\mu^2\lambda^2}\left(\frac{\delta_s}{\delta_n}\right)^2 - O\left(\frac{\delta_s}{\delta_n}\right)^3\right], \quad (36)$$

which yields a variation from $3K_n/2\lambda$, for vanishingly small asperity shear force, to 1.063 K_n/λ, for asperity shear force at incipient sliding condition.

Furthermore, it is noteworthy that the asperity sliding is accounted in accordance with equation (5). For example, the sliding domain under a normal deformation of the interface is given by $0 \le \phi \le 2\pi$ and $\theta_s \le \theta \le \pi/2a$, where θ_s = arctan $(\lambda\mu)$. For arbitrary shear loading conditions, the sliding domain is not known a priori, and an iterative numerical procedure is utilized to calculate the interface force-displacement relationship. In addition, for subsequent numerical study we admit the possibility of formation of new asperity contacts and loss of the existing contact due to separation as the interface is loaded. Thus the interface stiffness is obtained from

$$C^e_{ij} = N\int_0^r \int_0^{2\pi} \int_0^{\pi/2a} K^c_{ij}\, \xi(\phi,\theta) \sin\theta \, d\theta \, d\phi H(r)\, dr \qquad (37a)$$

$$C^p_{ij} = N\int_0^r \int_{\phi_s}^{} \int_{\theta_s} M^c K^c_{ik} \zeta^c_k K^c_{nj} q^c_m \xi(\phi,\theta) \sin\theta \, d\theta \, d\phi H(r)\, dr$$

$$+ N\int_0^r \int_{\phi_d} \int_{\theta_d} K^c_{ij}\, \xi(\phi,\theta) \sin\theta \, d\theta \, d\phi H(r)\, dr, \qquad (37b)$$

where $H(r)$ is asperity height distribution given by equation (12), $r = r_o + \delta_1$, and r_o is the asperity overlap at $\delta_1 = 0$.

4.1. Normal Force-Deformation Behavior

The normal displacement versus normal stress curves obtained from the present model are compared in Figure 11 with the experimental data on interfaces between Westerly granite blocks reported by *Yoshioka and Scholz* [1989a, b]. Solid lines give the calculated curves while the experimental data are indicated by symbols. The calculated curves were obtained using the following stiffness parameters: η = 0.5, K = 200 GPa $\mu m^{1/2}$, and λ = 1.2. These stiffness parameters are based on the Hertz-Mindlin stiffness parameters given in equation (34) for a shear modulus G = 20 GPa, Poisson's ratio ν = 0.3, and asperity radius of curvature R = 40 μm. The following asperity contact orientation parameters are assumed: a = 3 and b = c = 0 for the rough interface, and a = 6 and b = c = 0 for the smooth interface. The average asperity inclination, calculated as the expectation $E(\theta) = \int \theta\, \xi(\Omega)\, d\Omega$, is 19° for a = 3 and 10° for a = 6. The initial overlap r_o = 12 μm for the rough interface and 2 μm for the smooth interface, which is similar to the initial overlap reported by Yoshioka and Scholz. The asperity height distributions for the smooth and rough interfaces are given in Figure 3, and the contact density is taken to be $N = 10^{-2}$ μm^{-2}. The model correctly replicates a stiffer response as well as a greater displacement hardening for smooth interface. The stiffer response and displacement hardening of smooth interface is attributable to primarily two factors: (1) the narrow distribution of asperity heights which results in a rapid increase of the contact area due to the formation of new contacts and (2) the concentration of asperity contact orientation distribution toward the direction normal to the interface.

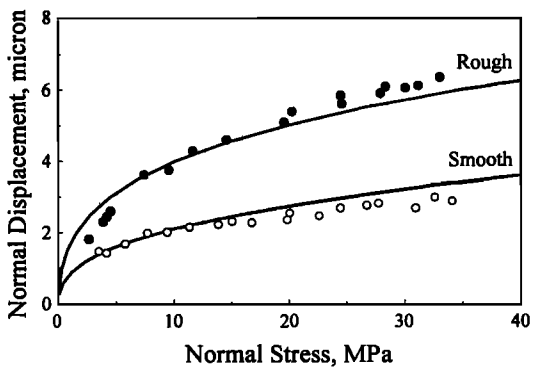

Figure 11. Comparison of measured and predicted interface normal behavior.

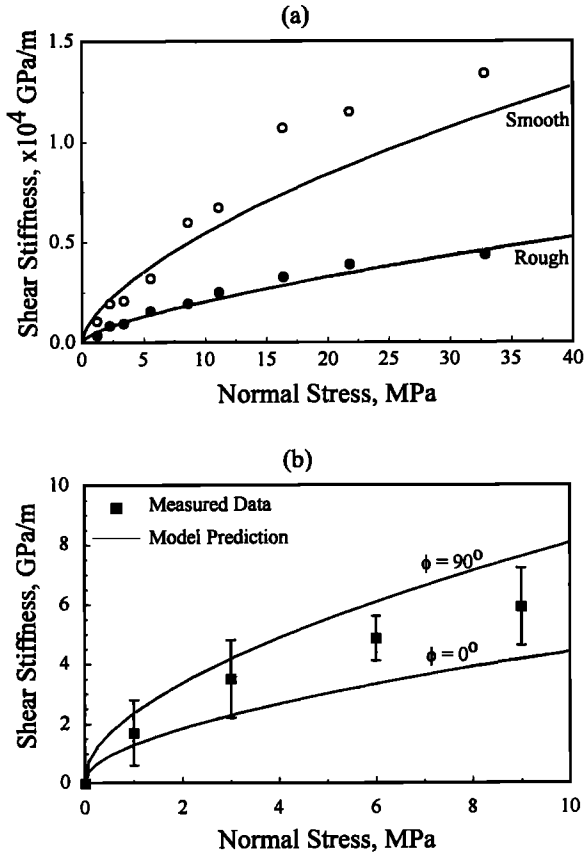

Figure 12. Comparison of measured and predicted initial shear stiffness versus normal stress for data from (a) *Yoshioka and Scholz* [1989b] and (b) *Jing et al.* [1992].

4.2. Initial Shear Stiffness Behavior

In Figures 12a and 12b we compare the initial shear stiffness calculated with the present model to the experimental data from *Yoshioka and Scholz* [1989b] and *Jing et al.* [1992], respectively. As in the case for normal stiffness the smooth interface has higher initial shear stiffness than the rough interface at a given normal stress. It is also observed that the initial shear stiffness increases nonlinearly with normal stress. The nonlinear behavior is attributable to the formation of new contacts as the normal stress is increased. Furthermore, a majority of the new contact formation occurs at relatively low normal stresses. Therefore the nonlinearity of the initial shear stiffness on normal stress diminishes at higher normal stresses.

From a comparison of Figures 12a and 12b it is observed that although the measured data has the same trends, the

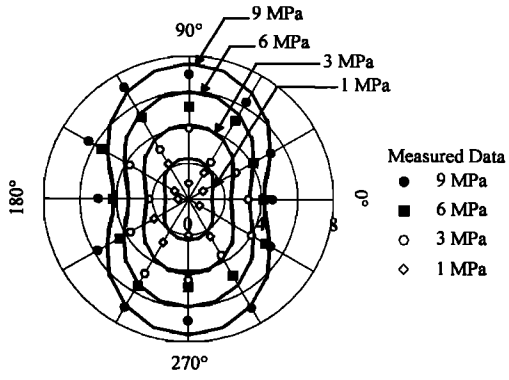

Figure 13. Comparison of measured and predicted directional dependence of initial shear stiffness for data from *Jing et al.* [1992].

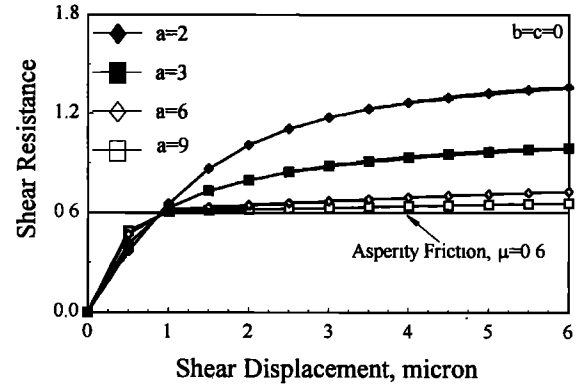

Figure 14. Effect of asperity orientation parameter a on interface shear resistance behavior.

values of initial shear stiffness reported by *Jing et al.* [1992] are considerably smaller than those reported by *Yoshioka and Scholz* [1989a]. Interestingly, this is a manifestation of the scale dependent nature of interface behavior. It is noteworthy that the tests by *Jing et al.* [1992] were performed using concrete replicas of rock joints. For these interfaces, the number of asperity contacts per unit area are expected to be larger as the sand used for making the concrete replicas has a mean grain radius of 15 mm. Jing et al. did not report any topography measurements. In absence of these measurements, for our calculations we use the parameters for smooth interface illustrated in Figure 3, with the modification that asperity heights and curvature are given in millimeters. The calculated curves in Figure 12b were obtained using the following values for asperity stiffness and contact orientation distribution parameters: $\eta = 0.5$, $K = 300$ GPa $\mu m^{1/2}$, $\lambda = 0.33$, $a = 3$, $b = -1$ and $c = -0.3$. The initial overlap for the interface is assumed to be $r_o = 3$mm. Solid squares and error bars, which give the maximum and the minimum value of shear stiffness at a given normal stress, show the measured data.

As reported by *Jing et al.* [1992], the spread in the shear stiffness measurements is a result of the anisotropic nature of the replicated interface. Figure 13 gives a directional plot of the measured interface shear stiffness along with the results of the present model. Although the measurements exhibit a considerable scatter, especially at low normal stresses, the present model captures the shear anisotropic behavior reasonably well.

4.3. Inelastic Behavior Under Shear Deformation

Under shear deformation of an interface, such that $\delta_1 \neq \delta_2 \neq \delta_3 \neq 0$, the asperity contacts can separate as well as slide. Therefore asperity separation as well as sliding contribute to the inelastic part of the stiffness tensor C_{ij}^P. In contrast to the case of normal loading, for shear loading, closed-form solutions that give the orientations of sliding and separating asperity contacts are complex and difficult to obtain. Numerically, the asperity separation may be detected by examining the total relative displacement in the normal direction of an asperity contact. The Amonton-Coulomb law discussed previously controls the sliding of an asperity contact, and the sliding occurs along the shear force at the asperity contact. The inelastic part of the interface behavior, in this case, may be obtained by numerically integrating equation (37b). Furthermore, for shear loading under controlled normal stress F_1 an iterative procedure is required to obtain the contact forces and displacements.

In Figure 14 we plot the shear resistance, given by F_2/F_1, versus the shear displacement for asperity orientation parameter $a = 2$, 3, 6, and 9 and $b = c = 0$. The asperity friction coefficient μ is taken to be 0.6 and asperity stiffness is assumed to be linear, i.e., $\eta = 0$, $K = 100$ GPa $\mu m^{1/2}$, and $\lambda = 1$. A normal displacement of $\delta_1 = 1$ μm is maintained during the shear loading given by $\delta_2 > 0$ and $\delta_3 = 0$. From Figure 14 it is seen that the asperity orientation parameter a has a significant effect on the interface frictional resistance. Furthermore, the interface friction tends toward asperity friction as a increases. It may be recalled that a higher value of asperity orientation parameter a indicates a smoother interface.

Figure 15 illustrates the effect of nonlinear asperity stiffness on interface shear resistance. Results for linear asperity stiffness are shown by solid squares and diamonds, and those for nonlinear asperity ($\eta = 0.5$, $\lambda = 1$) by open squares and diamonds. It is observed that interface with linear asperity exhibits a lower shear resistance than that with nonlinear asperity stiffness for the same initial normal loading condition. In addition, the effect is more pronounced for a rough surface with $a = 3$, than for a smooth surface with $a = 6$. Similar results are borne out from the simplified formulae of interface friction given by *Ford* [1993], which show that

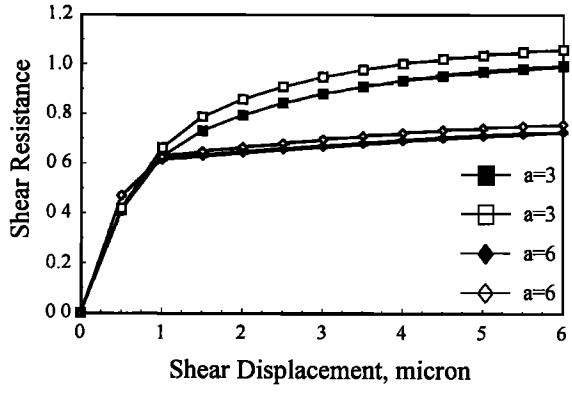

Figure 15. Effect of asperity nonlinearity on interface shear resistance behavior.

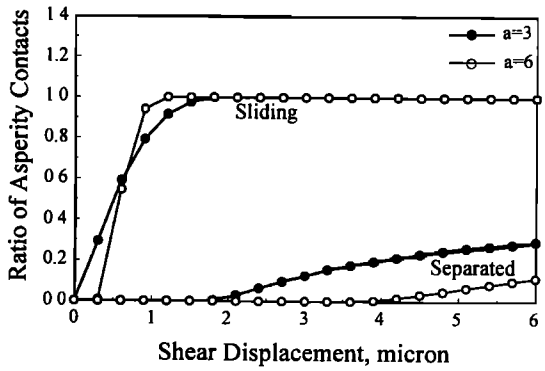

Figure 16. Evolution of sliding and separation of asperity contacts with shear displacement.

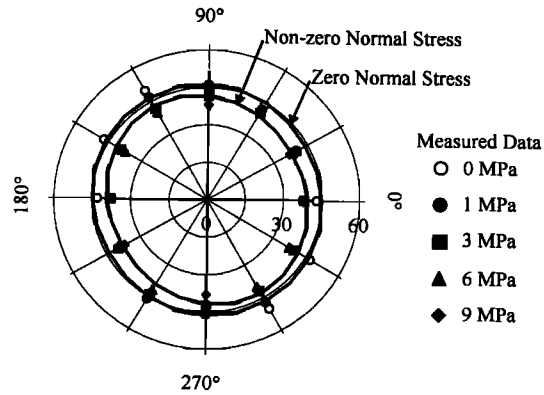

Figure 18. Comparison of measured and predicted directional dependence of interface friction for data from *Jing et al.* [1992].

linear asperity contacts have a lower effect of roughness upon shear resistance of an interface than nonlinear asperity contacts.

The evolution of sliding and separation of asperity contacts during shear loading is illustrated in Figure 16, which plots the ratio asperity contacts that are sliding or separated versus shear displacement. The ratio of asperity contacts is defined as the number of sliding or separated contacts divided by the total number of asperity contacts. In comparison to the rough interface (a = 3), the sliding at asperity contacts is mobilized at a lower shear displacement and a lower shear resistance for the smooth interface (a = 6). The asperity contact separation, on the other hand, commences at a higher shear displacement for the smooth interface. It is noted that for the smooth interface (a = 6), a larger number of asperity contacts are inclined in the direction normal to the interface, which expedites sliding at shear resistance close to the asperity friction coefficient while retarding the asperity separation. The average asperity inclination, calculated as the expectation $E(\theta) = \int \theta \xi(\Omega)\, d\Omega$, is 10° for a = 6 and 19° for a = 3.

In the above examples, asperity contact formation is not considered and asperity heights are taken to be uniform. To investigate the effect of asperity contact formation and asperity heights, we study the model performance by comparison with experimental results presented by *Biegel et al.* [1992] on interfaces between Westerly granite blocks. Experimental results show that a smooth interface, with a narrow distribution of asperity heights, exhibits higher shear resistance as well as deformation hardening before interface yield. Here interface yield is defined as the point at which the interface shear resistance changes drastically. In contrast, a rough interface, with a relatively broad distribution of asperity heights, has a lower shear resistance and deformation hardening. Although the behavior may seem counterintuitive, smooth interfaces exhibit higher shear resistance than rough interfaces because of a larger initial contact area under the same initial normal loading conditions. The present model correctly replicates this trend as illustrated in Figure 17. The model results were calculated using the following parameters: η = 0.5, K = 200 GPa $\mu m^{1/2}$, and λ = 1.2, which are based upon the Hertz-Mindlin stiffness parameters given in equation (34). The asperity friction coefficient, μ, is assumed to be 0.3. The following asperity orientation parameters are assumed: a = 2.5, b = 2.0, and c = 0 for rough interface and a = 3.0, b = 0.5, and c = 0 for smooth interface. The initial overlap r_o = 12 μm for the rough interface and 2 μm for the smooth interface. The asperity height distributions used in the calculations are given in Figure 3. A normal stress of F_1 = 10 MPa is maintained during the shear loading given by $\delta_2 > 0$ and δ_3 = 0.

As reported by *Jing et al.* [1992], the shear resistance of an interface may also exhibit anisotropic behavior. The measured directional dependence of shear resistance, expressed as friction angle $\tan^{-1}(F_2/F_1)$, for Jing et al. interface is plotted in Figure 18 along with the model predictions calculated for asperity friction coefficient of μ = 0.47. The calculated curves in Figure 18 were obtained using

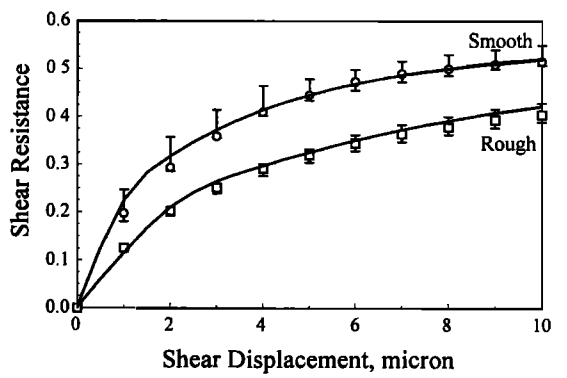

Figure 17. Comparison of measured and predicted interface shear resistance for data from *Biegel et al.* [1992].

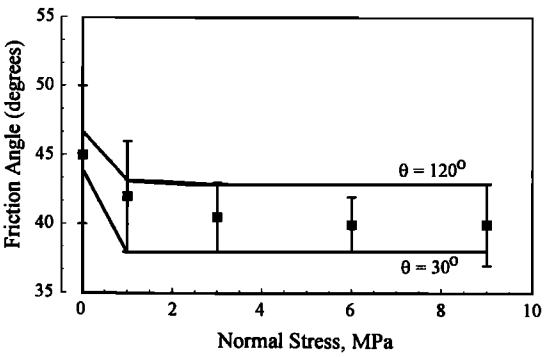

Figure 19. Comparison of measured and predicted interface friction versus normal stress for data from *Jing et al.* [1992].

the same parameters as those for Figure 12b. The present model readily replicates the anisotropy exhibited by the measured data. From Figure 18 it is also observed that the interface shear resistance is only minimally influenced by the interface normal stress. Predicted curves for nonzero normal stress are so close that they are indistinguishable. However, the friction angles at zero normal stress are predicted to be distinguishably larger. Similar observations are borne out from the measured data, which are shown by open circles for zero normal stress and filled circles, squares, diamonds, and triangles for nonzero normal stress in Figure 18. This observation is further exemplified in Figure 19, which gives the plot of interface shear resistance versus interface normal stress. From Figure 19 it is clear that the interface shear resistance for zero normal loads is higher than for nonzero normal load and that the normal stress has only a small effect on the interface friction angle.

5. Concluding Remarks

A micromechanical model of rough interfaces, such as rock joints, is developed by explicitly considering asperity interactions at the interface. In this context it is recognized that the interfaces often exhibit (1) anisotropic shear response and (2) deformation hardening of interface shear resistance under monotonic shear loading. To correctly account for these nuances in interface behavior, the composite surface topography of a rough interface is characterized via statistical distributions of asperity heights and asperity contact orientations. Gamma distribution is used for describing asperity heights, while a modified spherical harmonic expansion is introduced to model the asperity contact orientation distribution. Using this orientation distribution, the inelastic sliding and separation of asperity contacts are explicitly incorporated in the model.

The main result of this paper is derived in equations (22) and (23), which give the formulation for stiffness tensor of rough interfaces. The applicability of the derived formulation is then demonstrated by parametric studies of elastic and inelastic behavior of interfaces. Comparisons are also made with experiments.

Interface behavior studied with the derived model shows that the roughness of an interface is best characterized by distributions of asperity heights and asperity contact orientations. Closed-form expressions of interface elastic stiffness were obtained which show the variation of the relative effect of asperity normal and tangential stiffnesses with the interface roughness as described by the asperity contact orientations. These closed-form expressions may be used as a first approximation of rough interface stiffness in modeling jointed and granular materials.

Comparison with experimental data also suggests that the average values of asperity heights and asperity contact orientation may not be sufficient to capture all aspects of interface behavior. Asperity contact formation, as described by asperity height distribution, is important for distinguishing the smooth and rough interface stiffness behavior. Furthermore, the roughness of interface, as described by the asperity contact orientation parameters a, b, and c, has a significant effect on the shear stiffness and friction behavior of interface, as shown by deformation hardening and shear anisotropy.

Notation

a, b, c	parameters of $\xi(\Omega)$.
C_{ij}	interface stiffness.
f_i	asperity contact force.
F_i	interface force.
$H(r)$	asperity height distribution function.
K_{ij}	asperity contact stiffness.
N	number of asperity contacts per unit area.
r	asperity height.
R	asperity curvature.
α, β	parameters of $H(r)$.
δ_i	interface deformation vector.
δ_i^c	asperity contact deformation vector.
γ	magnitude of asperity contact inelastic deformation.
$\xi(\Omega)$	asperity contact orientation distribution.
Ω	solid angle.
θ, ϕ	spherical coordinates.
ζ_i	sliding direction.

References

Adler, R.J. and D. Firman, A non-Gaussian model for random surfaces, *Philos. Trans. R. Soc. London, Ser. A, 303,* 433-462, 1981.

Archard, J.F., Elastic deformation and the laws of friction, *Proc. R. Soc. London, Ser. A, 243*, 190-205, 1957.

Biegel, R.L., W. Wang, C.H. Scholz, G.N. Boitnott, and N. Yoshioka, Micromechanics of rock friction, 1, Effects of surface roughness of initial friction and slip hardening in Westerly Granite, *J. Geophys. Res., 97,* 8951-8964, 1992.

Boitnott, G.N., R.L. Biegel, C.H. Scholz, N. Yoshioka, and W. Wang, Micromechanics of rock friction 2. Quantitative modeling of initial friction with contact theory, *J. Geophys. Res., 97,* 8965-8978, 1992.

Bowden, F.P. and D. Tabor, *The Friction and Lubrication of Solids*, Clarendon, Oxford, England, 1950.

Brown, S.R. and C.H. Scholz, Closure of random elastic surfaces in contacts, *J. Geophys Res., 90,* 5531-5545, 1985.

Brown, S.R. and C.H. Scholz, Closure of rock joints, *J. Geophys. Res., 91,* 4939-4948, 1986.

Bush, A.W., R.D. Gibson, and T.R. Thomas, The elastic contact of a rough surface, *Wear, 35,* 87-111, 1975.

Bush, A.W., R.D. Gibson, and G.P. Keogh, Strongly anisotropic rough surface, *ASME Pap. 78-LUB-16,* Am. Soc. of Mech. Eng., New York, 1978.

Chang, C.S., and A. Misra, Packing structure and mechanical properties of granulates, *J. Eng. Mech , 116*(5), 1077-1093, 1989.

Chang, W.R., I. Etsion, and D.R. Bogy, An elastic-plastic model for the contact of rough surfaces, *J. Tribol., 109,* 257-263, 1987.

Ford, I.J., Roughness effect on friction for multi-asperity contact between surfaces, *J. Phys. D Appl. Phys., 26,* 2219-2225, 1993.

Francis, H.A., Application of spherical indentation mechanics to reversible and irreversible contact between rough surfaces, *Wear, 45,* 221-269, 1977.

Greenwood, J.A., and J.B.P. Williamson, Contact of nominally flat surfaces, *Proc. R. Soc. London, Ser. A, 295,* 300-319, 1966.

Hills, D.A., D. Nowell, and A. Sackfield, *Mechanics of Elastic Contacts*, Butterworth, Newton, Mass., 1992.

Jing, L., E. Nordlund, and O. Stephansson, An experimental study on the anisotropy and stress-dependency of the strength and deformability of rock joints, *Int. J. Rock Mech. Min. Sci. Geomech Abstr., 29,* 535-542, 1992.

Johnson, K.L., *Contact Mechanics*, Cambridge Univ. Press, New York, 1985.

Krolikowski, J., and J. Szczepek, Assessment of tangential and normal stiffness of contact between rough surfaces using ultrasonic method, *Wear, 160,* 253-258, 1993.

McCool, J.I., Comparison of models for the contact of rough surfaces, *Wear, 107,* 37-60, 1986.

McCool, J.I., and S.S. Gassel, The contact of two surfaces having

anisotropic roughness geometry, in *Energy Technology, Spec Publ Sp-7*, 29-38, Am. Soc. of Lubric. Eng., New York, 1981.
Mindlin, R.D., and H. Deresiewicz, Elastic spheres in contact under varying oblique forces, *J. Appl. Mech., 20*(3), 327-344, 1953.
Misra, A., Interfaces in particulate materials, in *Mechanics of Geomaterial Interfaces*, edited by A.P.S. Selavadurai and M.P. Boulon, pp. 513-536, Elsevier Sci., New York, 1995.
Misra, A., Mechanistic model for contact between rough surfaces, *J. Eng. Mech., 123*(5), 475-484, 1997.
Nayak, P.R., Random process model of rough surfaces, *J Lubr. Technol, 93,* 398-407, 1971.
O'Callaghan, M., and M.A. Cameron, Static contact under load between nominally flat surfaces in which deformation is purely elastic, *Wear, 36,* 79-97, 1976.
Swan, G., Determination of stiffness and other joint properties from roughness measurements, *Rock Mech. Rock Eng., 16,* 19-38, 1983.
Swan, G., and S. Zongqi, Prediction of shear behavior of joints using profiles, *Rock Mech. Rock Eng., 18,* 183-212, 1985.
Yamada, K., N. Takeda, J. Kagami, and T. Naoi, Mechanisms of elastic contact and friction between rough surfaces, *Wear, 48,* 15-34, 1978.
Yoshioka, N., A review of the micromechanical approach to the physics of contacting surfaces, *Tectonophysics, 277,* 29-40, 1997.
Yoshioka, N., and C.H. Scholz, Elastic properties of contacting surfaces under normal and shear loads, 1, Theory, *J. Geophys. Res., 94,* 17681-17690, 1989a.
Yoshioka, N., and C.H. Scholz, Elastic properties of contacting surfaces under normal and shear loads 2. Comparison of theory with experiment, *J. Geophys. Res., 94,* 17691-17700, 1989b.

A. Misra, Department of Civil Engineering, University of Missouri, 5110 Rockhill Road, Kansas City, MO 64110. (misraa@umkc.edu).

(Received November 10, 1998; revised May 17, 1999; accepted June 9, 1999.)